Progress In Electromagnetics Research C, Vol. 129, 187–201, 2023

Design of Wideband 8-Element MIMO Mobile Phone Antenna Based on Sub-6 GHz NR Band

Zhonggen Wang[1], Mingzhong Li[1, *], Ming Yang[2], Wenyan Nie[3], Weidong Mu[1], Han Lin[1], and Zhongyuan Lu[1]

Abstract—For the research of 5G NR band mobile phone bezel antenna, this paper proposes an 8-Element Multiple-Input Multiple-Output (MIMO) handset bezel antenna design for 5G New Radio (5G NR) bands. Moreover, the MIMO antenna's array is implemented by loading 8 identical antennas (Ant1–Ant8) into the metal bezel of the smartphone to form an 8-antenna array for a sub-6 GHz 8×8 MIMO system. In this setting, each antenna unit is a slot antenna type consisting of a Chinese character " "-shaped slot, as well as a 50 Ω micro-strip feeder; note that a satisfactory impedance matching is achievable in the upper-frequency band by loading a tuning stub on the feeder. The proposed 8-element antenna array covers 5G new radio (NR) band including N77 (3.3–4.2 GHz), N78 (3.3–3.8 GHz), N79 (4.4–5.0 GHz), and a Wi-Fi (2.4 GHz) band with a 10 dB impedance bandwidth. It is important to note that in addition to exhibiting ideal antenna efficiency and envelope correlation, the isolation between adjacent array elements is > 10 dB, and the peak gain is 3 dBi. In summary, the influence of the user's hand on the antenna is analyzed to ensure the robustness of the MIMO antenna system in practical applications.

1. INTRODUCTION

In recent years, with the development of social life, people's demand for information transmission rate has been constantly increasing. Therefore, modern communication systems nowadays must have a larger channel capacity, which promotes the development of 5G mobile communication. The 5th generation communication (5G) presents a faster data transmission speed and lower latency rate than the 4th generation communication (4G). Thus, according to the agreement, the data transfer rate of 5G is 100 times of that of 4G [1]. In this setting, MIMO antenna transmission technology effectively improves channel capacity and spectral efficiency and has become a key technology for multi-antenna operation. Moreover, MIMO technology has a wide range of applications in smartphone antennas, which increases its importance. However, the growing demand for higher data transfer rates with extremely low latency has led, eventually, to the introduction of 5th-generation New Radio (5G NR) communication systems. Reference [2] proposes a multi-input multi-output (MIMO) antenna suitable for 2.4 GHz and 5.8 GHz wireless local area network (WLAN). The frequency bands are 2.12–2.8 GHz and 4.95–6.65 GHz, but its efficiency is slightly insufficient. Reference [3] describes a human-face dual-polarized MIMO monopular patch antenna for ultra-wideband applications. The working frequency band is 2.8–16.1 GHz, and the coupling parameter of the working frequency band is less than −19.8 dB. However, the structure of the modified antenna is relatively complex. Reference [4] proposes a new prototype of eight-element

Received 16 December 2022, Accepted 1 February 2023, Scheduled 7 February 2023
* Corresponding author: Mingzhong Li (1228875294@qq.com).
[1] School of Electrical and Information Engineering, Anhui University of Science and Technology, Huainan 232001, China.
[2] Department of Electrical and Communications Engineering, West Anhui University, Lu'an 237012, China. [3] School of Mechanical and Electrical Engineering, Huainan Normal University, Huainan 232001, China.

MIMO antenna system for 5G communication, Internet of Things and network. The isolation is less than −12 dB, but the antenna operates in a band of 3.4 GHz to 3.6 GHz with narrow bandwidth.

In this context, according to the 3G Cooperation Project Technical Specification 38.101, the 5G NR frequency bands are subdivided into frequency band one (FR1) and frequency band two (FR2). The former is a 5G NR band that operates in the sub-6 GHz (or sub-6 GHz band), while the latter is a 5G NR band operating in mm wave [5]. In the sub-6 GHz frequency band, at present, 3G/4G mobile communication systems use frequency bands operating below 3 GHz, while frequencies between 5 and 6 GHz are used in the WLAN 5-GHz band (5150–5825 MHz). Subsequently, 5G NR bands N77 (3300–4200 MHz), N78 (3300–3800 MHz), and N79 (4400–5000 MHz) are planned for 5G networks. References [6–8] are the research on the mobile antenna of 5G NR band in recent years, which have some problems in broadband and isolation degree.

At present, multiple 5G smartphone MIMO antenna array designs from the single-band type do exist, operating in the C-band 3400–3600 MHz or as part of the bandwidth of 5G NR band N78. All of the References [9–16] address the above frequency bands. These designs consist entirely of antenna models composed of 8 to 12 antenna array elements; various antenna design techniques have been suggested, such as inverted-F, a monopole antenna, and loop antennas. In particular, slot antennas have been further developed recently. In this setting, References [17–24] present all slot antennas used in 5G communication. Moreover, they have the advantages of simple structure, easy integration of active devices, and wide operating frequency band. Nevertheless, when these antennas are employed in 5G NR bands, significant improvements in bandwidth utilization are yet to be made. Reference [25] proposes a dual-band optically transparent antenna based on a slotted interconnected ring resonator as an efficient radiating element, and the radiation disadvantage of over the air (OTA) due to the low conductivity of conductive oxides has been overcome with the gain improvement technique of 2×1 antenna array design.

Furthermore, the coupling between antenna elements is a major issue that affects the performance of MIMO systems. Hence, multiple decoupling techniques have been proposed in MIMO antennas in recent years, such as defect-grounded structures [26], orthogonal polarization [27], and and neutralization lines [28]. Moreover, self-decoupling techniques [29–31] have been studied to further enhance isolation. In this context, these decoupling techniques provide the basis for improved isolation in MIMO systems.

In this study, an 8-element MIMO cell phone bezel antenna for the 5G New Radio (5G NR) band is suggested, covering the 5G NR band, N77/N78/N79 band, and Wi-Fi (2.4 GHz) band with better performance isolation. On this basis, the method of metal plate slotting is adopted, and 2 open branches are added in the middle of the original Z-shaped slot, to improve the impedance matching characteristics and form a “ ” slot antenna. Consequently, the optimized slot antenna has a bandwidth of 3.3 GHz to 5.10 GHz, as well as an envelope correlation coefficient (ECC) inferior to 0.01.

The remainder of this study is structured as follows. The second section discusses the design process and working mechanism of the MIMO antenna system, including the design structure, parameter analysis, and working principle. Section 3 presents the antenna fabrication, simulation results, measured environment, and measured results of the proposed MIMO system, while in Section 4, the influence of human body structure on the antenna performance is discussed, including the single-handset mode (SHM) and dual-handset mode (DHM). Furthermore, in Section 5, a comparison is made through a comparison chart that highlights the advantages of the proposed design. Finally, the conclusion is drawn in Section 6.

2. PROPOSED MIMO ANTENNA SYSTEM

2.1. Antenna Geometry

Figure 1(a) shows a model of the antenna system with the antenna elements positioned on the phone's metal frame and ground plane. In this setting, the entire antenna system consisted of four vertical metal frames on the system substrate (the bottom was the ground plane). Note that the system substrate material was FR ($\varepsilon_r = 4.4$ and $\tan\delta = 0.02$), and the dimensions were “150 mm × 70 mm”. Moreover, the metal frames were 7 mm high and made from FR4; they are positioned around the system substrate surrounding the ground. The proposed 8-antenna array (Ant1–Ant8) was subdivided into two 4-antenna sub-arrays (Ant1–Ant4 and Ant5–Ant8) that were set on metal frames on the left and right long sides,

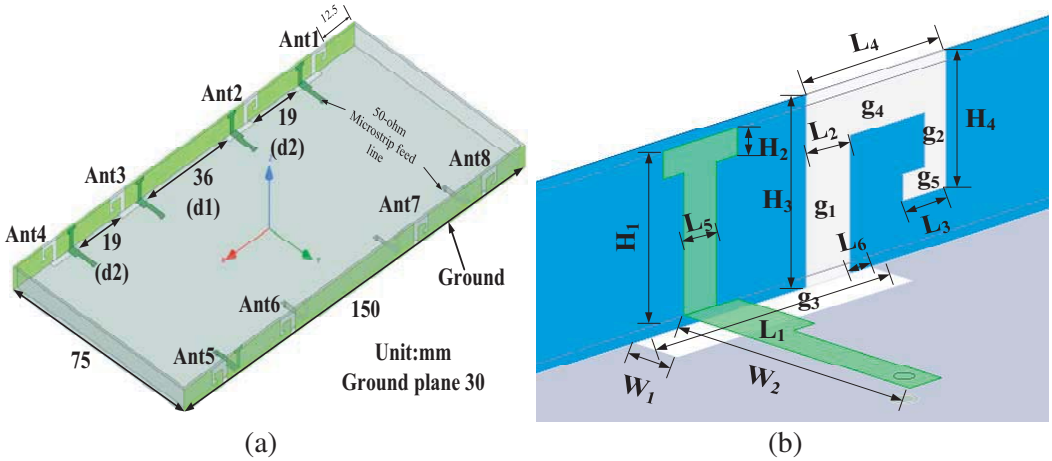

Figure 1. Geometry and dimensions of the proposed MIMO antenna system. (a) Perspective view. (b) Detailed structure of the slot antenna element (Ant1).

where Ant1–Ant4 were symmetrical with Ant5–Ant8. For brevity, this study only discusses Ant1–Ant4. Two 75 mm × 12.5 mm clearance areas (located at the top and bottom of the smartphone) were reserved for 3G/4G/WLAN antennas, etc. In order to further achieve satisfactory impedance matching, an ideal envelope correlation coefficient (ECC) is given, which is a key index to evaluate the performance of MIMO radiation mode. Basically, if the polarization directions of the two antennas are perpendicular to each other, then the ECC is zero. When acting alone, the smaller the ECC value is, the smaller the influence of antenna interaction is. Ant1-Ant2 and Ant3-Ant4 are structurally symmetrical, which improves the degree of isolation between antenna units. Furthermore, the distance ($d1$) between Ant2 and Ant3 was 36 mm, while the distance ($d2$) between Ant1 and Ant2 (Ant3 and Ant4) was 19 mm. Table 1 lists the proposed optimal parametric sizes for MIMO antennas.

Table 1. Optimized parametric dimensions of proposed MIMO antenna (unit: mm).

L_1	L_2	L_3	L_4	L_5	L_6
11	2	2	6.5	1.5	2
W_1	W_2	H_1	H_2	H_3	H_4
2	10.5	6.2	1	7	5

Figure 1(b) depicts the detailed geometry and dimensions of the proposed single antenna element (Ant1). As shown, the " " shaped opening slot consisted of two vertical slots (dimensions 7 mm × 2 mm loaded on a standing metal frame) and three horizontal slots (dimensions 9 mm × 2 mm loaded in a ground edge aircraft). The vertically slotted $g1$ (subsequently simplified as $g1$) and $g2$ were mounted on a metal frame, with $g1$ measuring 7 mm × 2 mm and $g2$ measuring 5 mm × 1 mm. The horizontal slot $g3$ was mounted on the ground plane and measured 11 mm × 2 mm, while the horizontal slots $g4$ and $g5$ were mounted on the metal frame; $g4$ was 3.5 mm × 2 mm and $g5$ 1 mm × 1 mm. It is worth noting that if the " " type slot was mainly loaded on the metal frame and did not involve the ground plane, it would have been difficult to achieve broadband operation (will be explained in detail later in the study). As for the 50 Ω microstrip feeder, it consisted of a horizontal section and a vertical section. The horizontal part was printed on the upper surface of the system substrate, which consisted of a rectangle with a size of 10.5 mm × 1.5 mm and a rectangle measuring 3.6 mm × 1 mm. The vertical part was made up of a "T-shaped" metal strip.

2.2. Design and Corresponding Analysis

As shown in Fig. 1(b), two open branches $g2$ and $g5$ are added to the original bending structure composed of $g1$, $g3$, and $g4$ to form a " " shaped structure. To illustrate the effect of the branches on the performance of the antenna element, an in-depth study of the proposed array antenna was conducted, by means of the commercial software ANSYS high-frequency structure simulator. In Fig. 2(a), a comparison was made between the S-parameters of the antenna element with no added branches to the antenna element with added branch $g2$, and the antenna element with added branches $g2$ and $g5$. As can be seen in the figure, with and without an increased understanding that these two branches affect the impedance matching and operating bandwidth elements of a single antenna array, the parametric study was only performed on Ant1 (other antennas were removed). In this setting, when branch $g2$ was not added, the impedance matching of the antenna elements was poor. After adding branch $g2$, the impedance matching of the antenna element was obviously improved, and the bandwidth was between 3.03 and 5.2 GHz. After adding branches $g2$ and $g5$, the antenna elements achieved outstanding impedance matching, and the measured reflection coefficients verified that the proposed 8-antenna array covered 5G NR bands N77/N78/N79 and Wi-Fi bands (2.4 GHz) in a satisfactory manner.

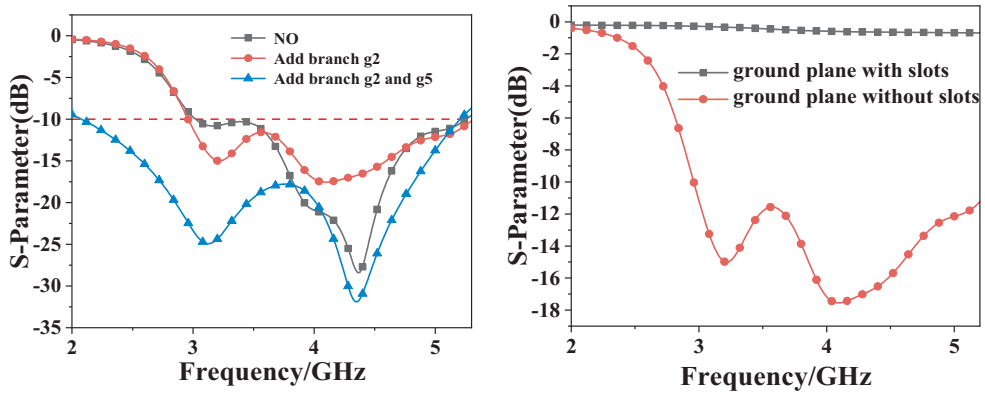

Figure 2. Evolution process of antenna element structure. (a) Simulated reflection coefficients of branch. (b) S-parameter plot of ground plane with and without slots.

Furthermore, the influence of the " "-shaped slot on the broadband was analyzed to determine whether the ground plane is with slots. In Fig. 2(b), it is clear that when the ground plane is without slots, the bandwidth is almost nonexistent. On the other hand, when the ground plane is with slots, the bandwidth increases significantly. This is because the antenna achieves good impedance matching when the slot involves the ground, thus expanding the bandwidth.

2.3. Proposed Antenna Design

The proposed 8-element antenna array has been fabricated, and its actuality is shown in Figs. 3(a) and (b). The proposed 8-port MIMO antenna system was simulated using the ANSYS software, and its S-parameters were determined using a vector network analyzer. Far-field testing was performed in an anechoic microwave chamber. The corresponding results are presented and discussed in the following sections.

3. RESULTS AND DISCUSSION

3.1. S-Parameters

As shown in Figs. 4(a) and (b), the antenna model was measured in an anechoic chamber to obtain its actual reflection coefficient and isolation. Since the 8-element array antenna was symmetrically

(a) (b)

Figure 3. Fabricated prototype. (a) Front view. (b) Top view.

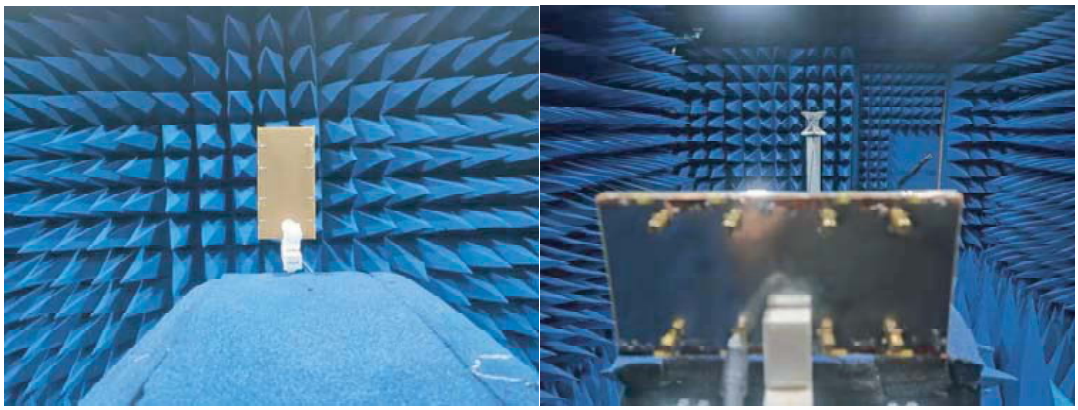

(a) (b)

Figure 4. Antenna model anechoic chamber measurement diagram. (a) Front view. (b) Back view.

distributed on the metal frame on both sides, the simulated and measured S-parameter values of only one side were given here. Moreover, as shown in Fig. 5(a), there is a certain difference between the simulated and measured reflection coefficients. The actual measured resonant frequency point is slightly shifted to the right compared to the simulated one. For example, in the simulation results of S_{11}, its resonant frequency is 2.8 GHz; the actual measured resonant frequency is 2.9 GHz; its corresponding reflection coefficient is from 2.01–5.23 GHz into 2.03–5.21 GHz, indicating that the actual effect of manufacturing needs to be improved. These differences may be due to the manufacturing process or measurement errors. Furthermore, it can be seen from the figure that the impedance bandwidth of Ant2 and Ant3 is slightly inferior to that of Ant1 and Ant4 because they are close to the middle part of the ground plane, sandwiched between the two antennas. However, the actually measured reflection coefficients cover the 5G NR bands N77/N78/N79 and the WiFi band (2.4 GHz) in a good manner. Fig. 5(b) presents the simulated quantity of the transmission coefficient, and Fig. 5(c) denotes the actually measured quantity of the transmission coefficient. In terms of isolation degree, the measured results are inferior to those achieved by simulation. For example, the S_{12} obtained by simulation is -12 dB, while the measured S_{12} is -11.5 dB. It can be seen from the figure that the difference between the analog quantity and measured quantity is not very obvious, mainly because of the measurement accuracy. However, the measured results show that the isolation between adjacent ports is superior to 10 dB, indicating that the port multiplexing performance is satisfactory and meets the MIMO antenna communication standard.

3.2. Radiation Performance

In general, a mobile terminal has a favorable orientation map. Fig. 6 presents the XOZ and YOZ plane orientation diagrams of Ant1–4. It can be seen in the figure that when XOZ is used as the radiation plane, the higher radiation gain directions of Ant1–4 are around 90° and 270°, and their peak gains

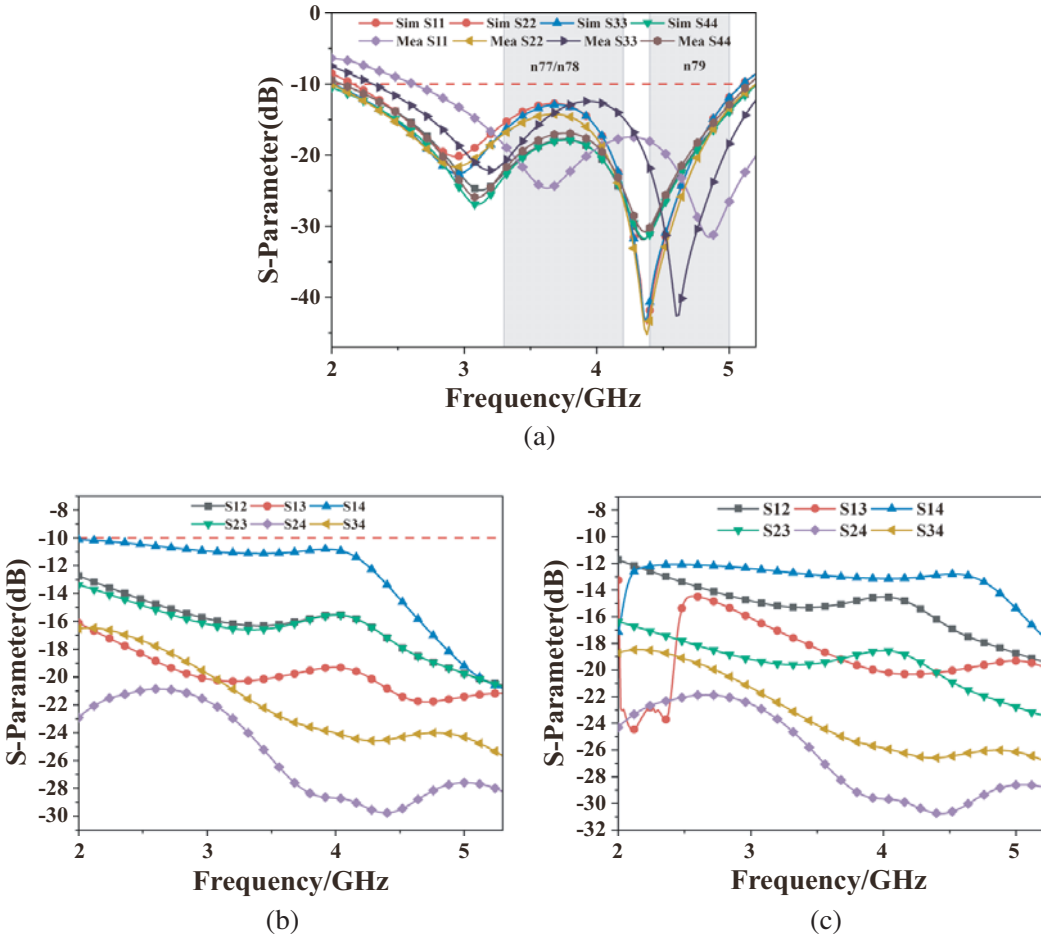

Figure 5. *S*-parameters. (a) Simulated and measured reflection coefficients. (b) Simulated transmission coefficients. (c) Measured transmission coefficients.

all exceed 3 dBi. On the contrary, when the YOZ plane is employed as the radiation plane, Ant1–4 have higher radiation gains in all directions. The maximum radiation direction of Ant1–4 is around 0 degrees, and the corresponding gain obtained from the test is 0 dBi, 2.5 dBi, 3 dBi, 2.3 dBi, respectively. Due to the mirror image distribution of the antenna elements, the antenna radiation directions are complementary, resulting in distinguished far-field radiation characteristics.

Figure 7 illustrates the simulated and measured overall efficiencies of the antenna system. It is clear from the figure that the actual measured efficiency is not much different from the simulated efficiency result. Hence, the total efficiency of the simulated and actually measured operating bandwidth is between 55% and 75%, which is about 20% lower than the simulated value. More significantly, at the resonant frequency, the measured value reached more than 65%, and the radiation efficiency reached more than 70% in the 4.4–5 GHz frequency band. Nonetheless, all measured total efficiencies are more than 55%, indicating that high antenna efficiencies are achieved.

4. DIVERSITY PERFORMANCE

The excellent diversity characteristics of MIMO antennas provide an improved anti-fading and anti-jamming performance, allowing each antenna to operate independently. In this section, the diversity performance of the proposed MIMO antenna will be introduced and studied in detail from the aspects of envelope correlation coefficient (ECC), total active reflection coefficient (TARC), mean effective channel gain (MEG), and diversity gain (DG).

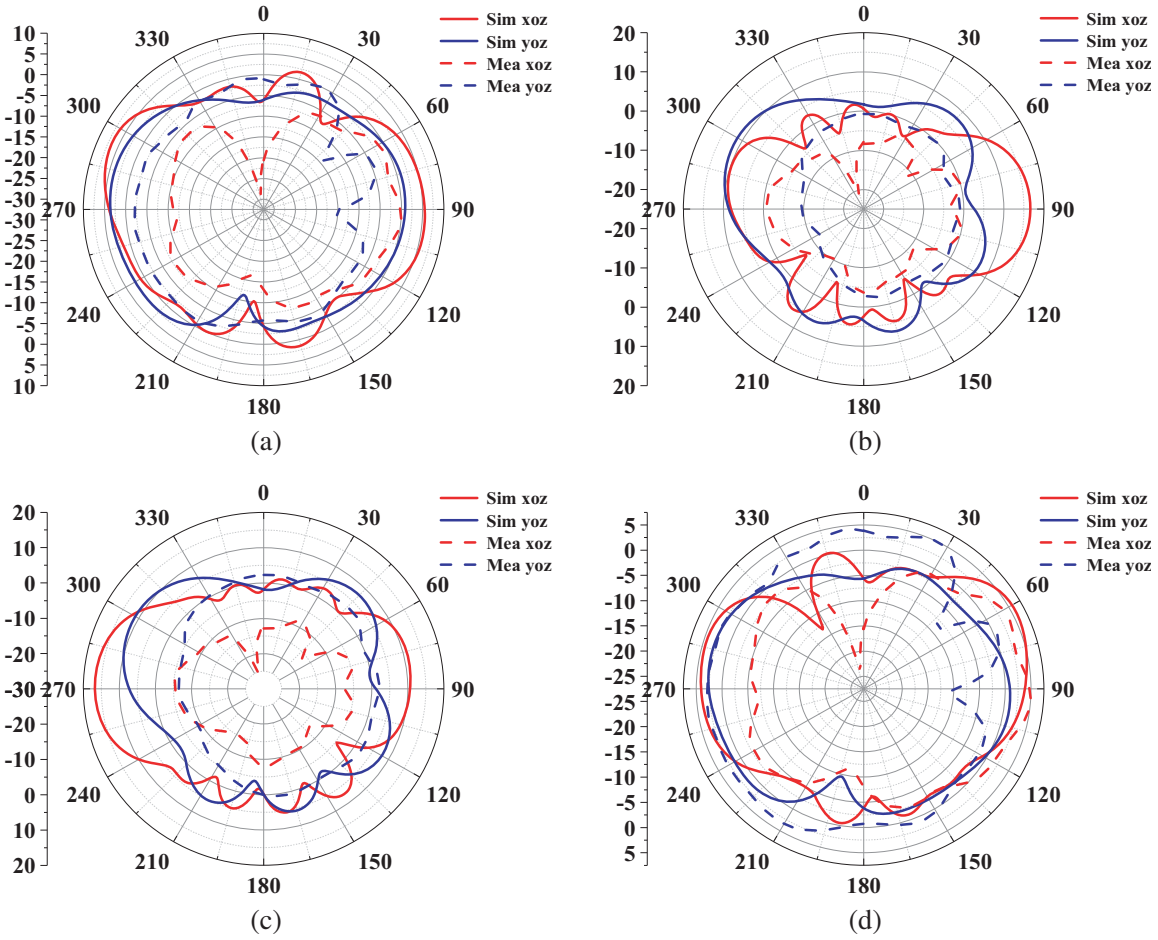

Figure 6. Simulated and measured radiation patterns. (a) Ant 1 XOZ and YOZ. (b) Ant 2 XOZ and YOZ. (c) Ant 3 XOZ and YOZ. (d) Ant 4 XOZ and YOZ.

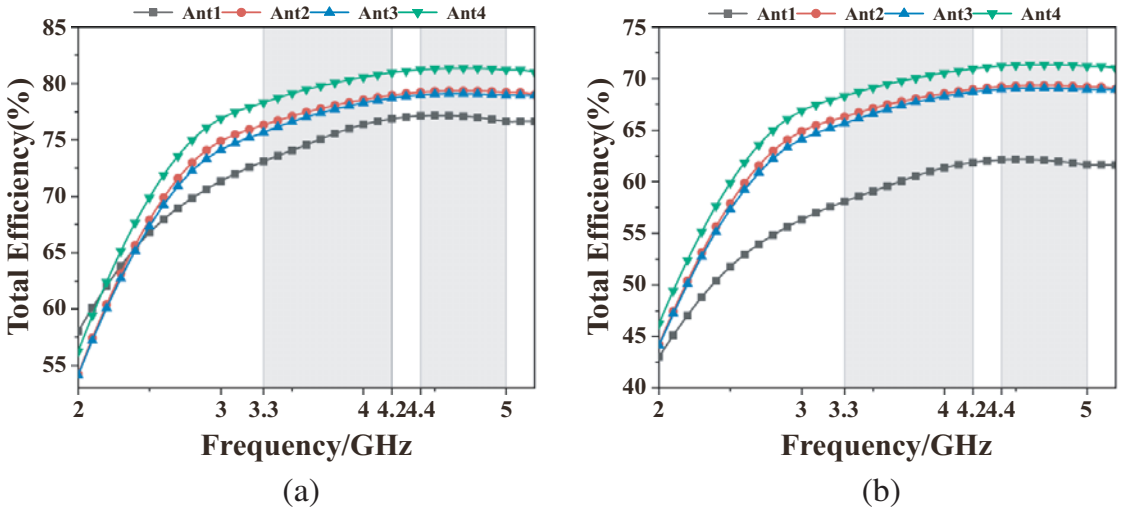

Figure 7. Total efficiency. (a) Simulated efficiency. (b) Measured efficiency.

4.1. Envelope Correlation Coefficient (ECC)

A crucial indicator for assessing how well MIMO antennas operate in terms of radiation pattern diversity is the envelope correlation coefficient (ECC). In this setting, the value of ECC indicates the quality of the antenna correlation. Subsequently, lower ECC values indicate a superior MIMO system performance since they are correlated with lower levels of mutual coupling, as well as fewer influences of each antenna on the others when operating independently. Note that modern mobile terminals require MIMO antennas to have an ECC lower than 0.5. The calculation's equation is as follows [32]:

$$\mathrm{ECC} = \frac{\left|S_{ii}^{*}S_{ij} + S_{ji}^{*}S_{jj}\right|^{2}}{\left(1 - |S_{ii}|^{2} - |S_{ji}|^{2}\left(1 - |S_{jj}|^{2} - |S_{ji}|^{2}\right)\right)} \tag{1}$$

As illustrated in Fig. 8, the ECC values are lower than 0.01. Across the operation bandwidth, the largest ECC (between Ant1 and Ant2) is only 0.00616. Accordingly, when the resonant frequency is 3.2 GHz, the corresponding maximum ECC value is 0.00241.

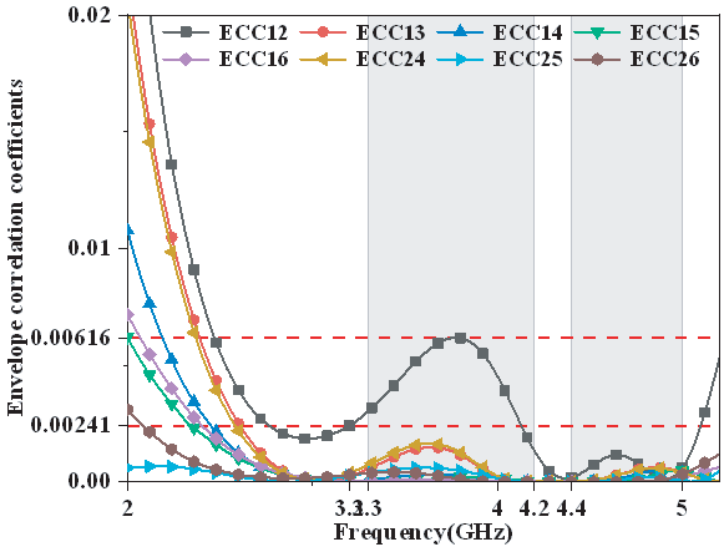

Figure 8. Calculated ECCs.

4.2. Total Active Reflection Coefficient (TARC)

In MIMO systems, the measured TARC is related to the total reflected power and total incident power. Ideally, TARC should be zero, which means that the antenna receives all incident power [33]. The measurement of TARC is crucial because it can determine the effectiveness of the MIMO system. For a two-port system, TARC can be calculated by Equation (2) [34]. The calculated TARC of the proposed MIMO antenna is shown in Fig. 9, which indicates that the calculated TARC is lower than −30 dB in the operating frequency band.

$$\mathrm{TRAC} = -\sqrt{\frac{(S_{11} + S_{12})^{2} + (S_{21} + S_{22})^{2}}{2}} \tag{2}$$

4.3. Mean Effective Gain (MEG)

MEG is another important parameter to characterize the multi-party function, that is, the ratio of the average received power to the average incident power. The ideal value is about ±3 dB. If for $3|\mathrm{MEG}_1/\mathrm{MEG}_2| < \pm 3\,\mathrm{dB}$ values, say MIMO system will get a good diversity performance [35]. The

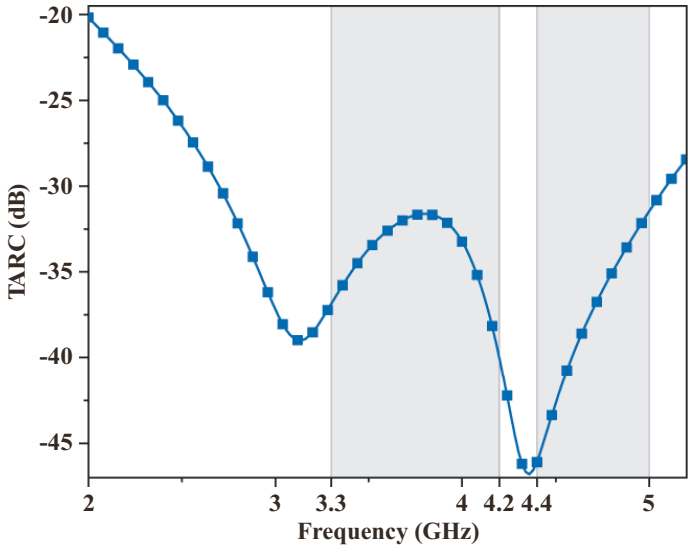

Figure 9. Total active reflection coefficient.

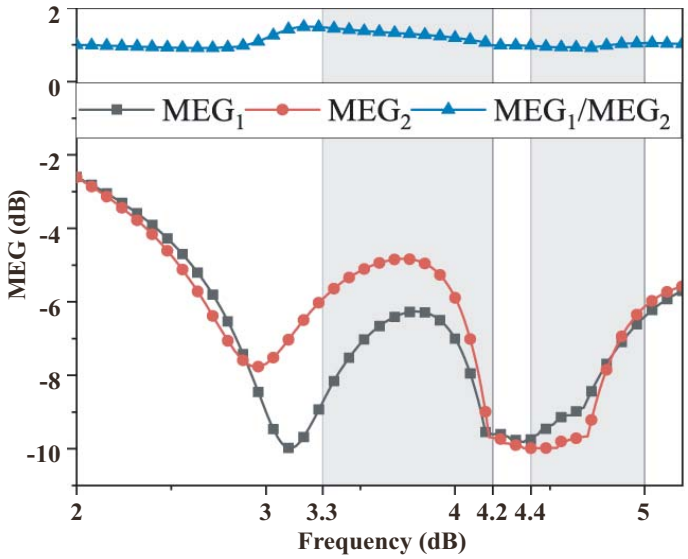

Figure 10. Mean effective gain.

calculation results are calculated by Equations (3) and (4), as shown in Fig. 10. It is clear that these results are still satisfactory.

$$\mathrm{MEG}_1 = 0.5\left[1-|S_{11}|^2-|S_{12}|^2\right] \tag{3}$$

$$\mathrm{MEG}_2 = 0.5\left[1-|S_{12}|^2-|S_{22}|^2\right] \tag{4}$$

4.4. Diversity Gain (DG)

Diversity gain (DG) is a measure of how beneficial diversity is. Within the operating frequency range, the optimal value of DG to achieve acceptable reliability of wireless communication systems is about 10 dB [36]. Using the ECC value, DG can be determined from Equation (5) [37]. Similarly, Fig. 11 depicts the calculated DGs of the antenna, where it can be observed that the DGs of the MIMO antenna

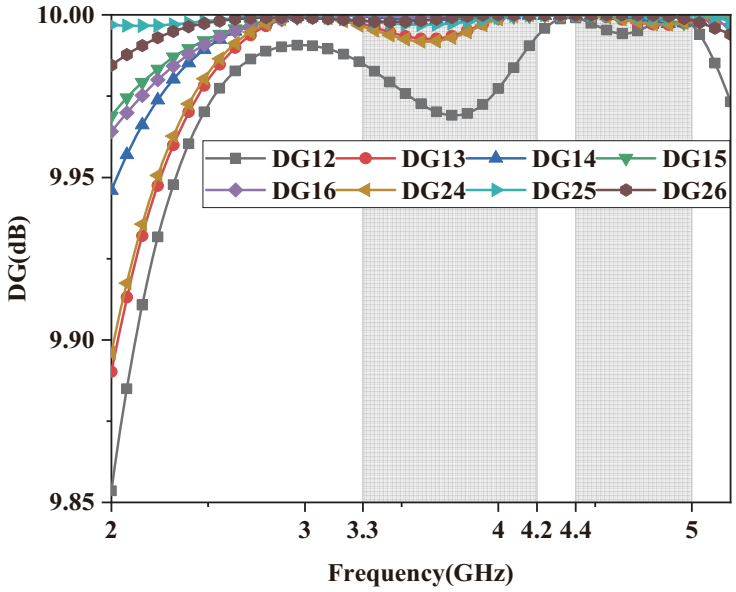

Figure 11. Diversity gain.

are about 10 dB in the operating band.

$$\mathrm{DG} = 10 \times \sqrt{1 - |\mathrm{ECC}|} \tag{5}$$

5. PRACTICAL APPLICATION ANALYSIS

The impact of realistic antenna performance is covered in this section. The single handset mode (SHM) and double handset mode (DHM) are the two most commonly used operation modes. Fig. 10 depicts the simulated application scenario. The effect on the user's head will not be discussed here, as the operation is employed exclusively for data transmission, not for call mode.

As shown in Fig. 12(a), Ant7 is in direct contact with the finger while Ant4 and Ant8 have a certain distance from the finger. Fig. 13 illustrates the reflection coefficient, transmission coefficient, and radiation efficiency of the antenna system under SHM. It is known from Fig. 13(a) that the reflection coefficient of Ant7 is low, and the bandwidth drops to 2.5–5.0 GHz. In contrast, the reflection coefficients

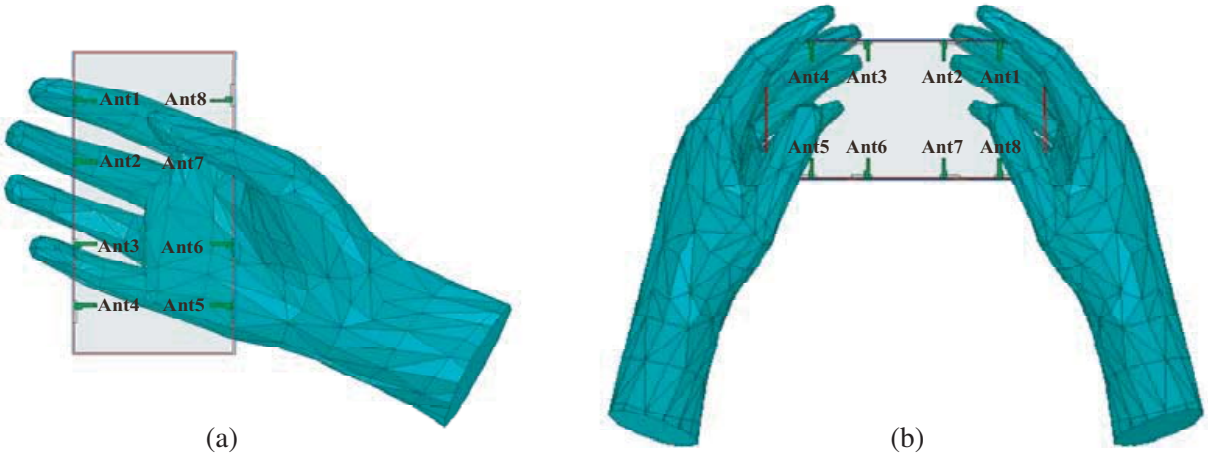

Figure 12. Two application scenarios of a hand-held smartphone. (a) SHM. (b) DHM.

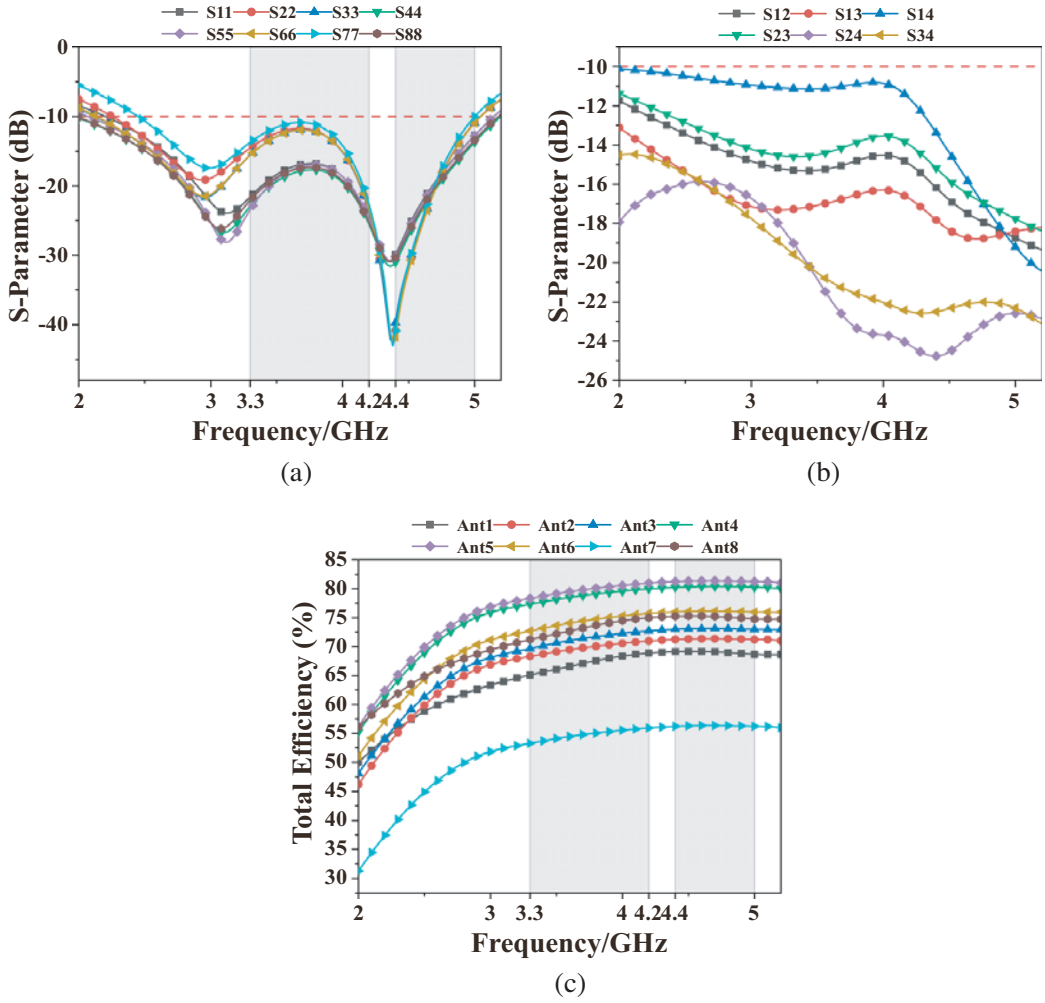

Figure 13. Simulated parameters under SHM. (a) Reflection coefficient. (b) Transmission coefficient. (c) Total efficiency.

of Ant1, 2, 3, 5, and 6 are slightly less affected, and the bandwidths below −10 dB can still contain 2.2–5.1 GHz because of their distance from the finger. Nevertheless, the 3.3–5.1 GHz band is still covered. It is clear from Fig. 13(b) that the isolation degree between antenna units 1 and 4 is less than −10.2 dB, and the isolation degree between other antenna units is less than −11 dB. It can be seen that the transmission coefficient between antenna units is slightly higher than that without hand interference, and the isolation in the working frequency band is still better than 10 dB. As shown in Fig. 13(c), the radiation efficiency of Ant7 is reduced to below 55% due to the electromagnetic wave absorption by hand tissue. Moreover, Ant1, 2, 3, 5, and 6 are about 18% less efficient due to their proximity to the palm, in contrast to Ant4 and Ant8 which are farther from the hand and are more than 75% efficient.

As for DHM, only Ant5 and Ant8 are in direct contact with the finger, as shown in Fig. 12(b) while all other antenna elements are not in direct contact with the fingers. Fig. 14 shows the reflection coefficient, transmission coefficient, and radiation efficiency of the antenna system under DHM. As shown in Fig. 14(a), since Ant5 and Ant8 are covered by thumb, their reflection coefficients increase significantly. The resonant frequency of Ant5 becomes 3.1 GHz, and that of Ant8 becomes 3.15 GHz. The resonance point moves to the right, resulting in significantly poor impedance matching. While their resonant frequencies are not remarkably different from those of the other antenna elements, their impedance matching is also worse than that without interference. In contrast, other antenna elements are not highly affected. As shown in Fig. 14(b), the transmission coefficient between antenna units 1 and

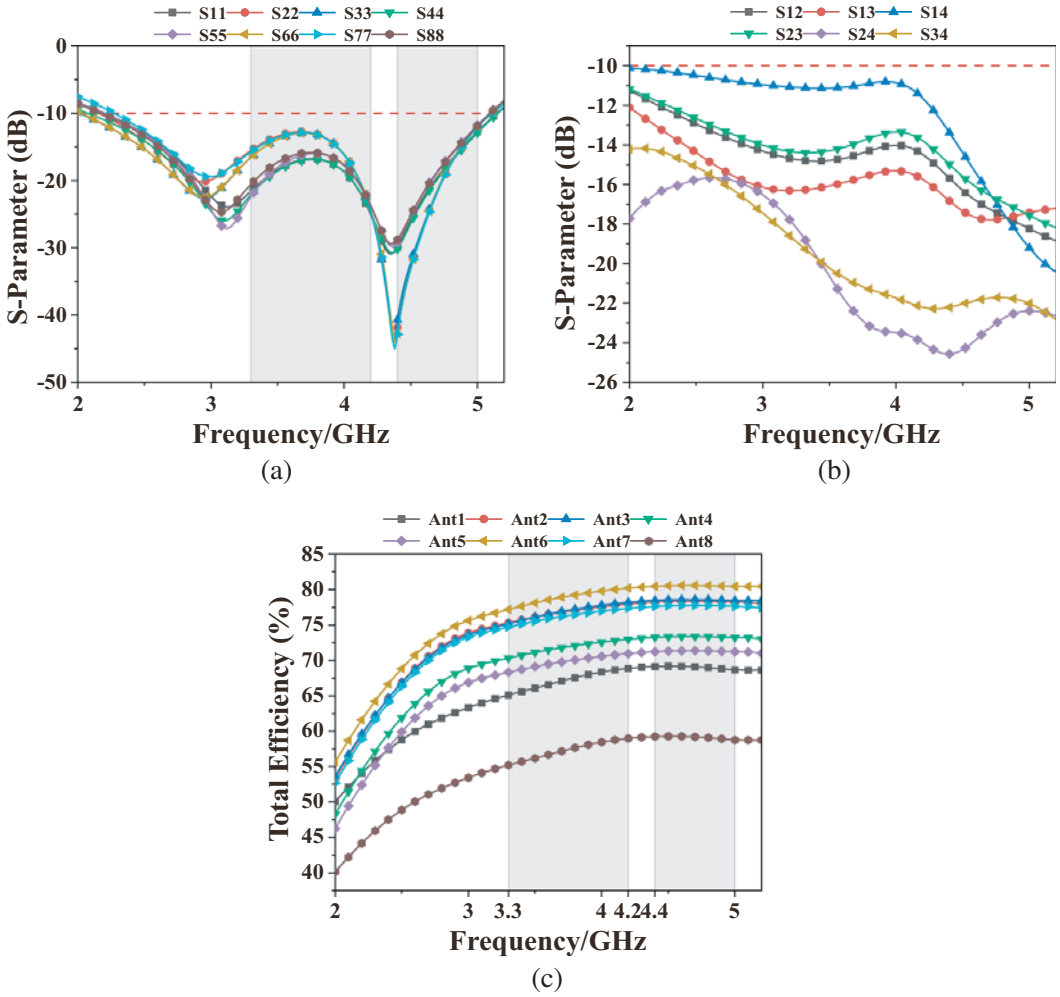

Figure 14. Simulated parameters under DHM. (a) Reflection coefficient. (b) Transmission coefficient. (c) Total efficiency.

4 increases significantly, and the isolation performance is below 10.1 dB. The transmission coefficient between antenna units 3 and 4 increases slightly, and the isolation performance is below −11 dB. The transmission coefficient between antenna units 1 and 2 increases slightly, and the isolation performance is below −11 dB. However, a good isolation performance of more than 10 dB is still maintained between the ports. As depicted in Fig. 14(c), the radiation efficiency of these antenna elements, which are not in contact with the fingers or palm, remains more than 70% over the entire operating bandwidth. In contrast, Ant5 and Ant8 experience a significant drop in efficiency when being in contact with fingers, with a maximum efficiency of only around 50%.

6. COMPARISON AND DISCUSSION

To illustrate the advantages of the proposed antenna array, Table 2 compares the suggested work with several previously introduced designs. As shown in this table, when the resonant frequency is 2.8 GHz, the bandwidth of the proposed array is 2.03–5.21 GHz, which is wider than that of the previous arrays. Furthermore, when the resonant frequency is 2.8 GHz, the isolation degree of the proposed array is less than −10 dB, and the suggested design achieves satisfactory isolation. In terms of overall efficiency, bandwidth limitations are overcome at a lower cost. Since it enables broadband and spatial multiplexing, it is an outstanding candidate for 5G NR communications.

Table 2. Performance comparison of 5G antenna array.

References	Bandwidth (GHz)	Isolation (dB)	ECC	Total Efficiency (%)	Discussion
[10]	3.4–3.6 (−10 dB)	> 10	< 0.2	62–78	High efficiency but narrow bandwidth
[11]	3.4–3.625 3.90–4.55 (−10 dB)	> 20.1	< 0.3	> 40	Isolation degree is high, but slightly lower efficiency
[15]	3.4–3.6 (−6 dB)	> 14	< 0.15	40–52	ECC has good performance but narrow bandwidth
[16]	3.4–3.6, 4.8–5.1 (−6 dB)	> 11.5	< 0.08	40–83	Dual frequency band is efficient, but the bandwidth is narrow
[18]	3.3–3.9 (−6 dB)	> 15	< 0.01	40–52	ECC has good performance and isolation degree is high, but narrow bandwidth
[19]	3.4–3.6 (−10 dB, 5G modules)	> 12	< 0.02	> 60	ECC has good performance but narrow bandwidth
[24]	3.39–3.67 (−10 dB)	> 17.5	< 0.036	62–76	Isolation degree is high, but narrow bandwidth
proposed	2.03–5.21 (−10 dB)	> 10	< 0.01	72–75	Wide belt, high efficiency

7. CONCLUSION

This study presents an 8-element MIMO handset bezel antenna design for 5G New Radio (5G NR) bands. In this context, the MIMO antenna array is implemented by loading eight identical antennas (Ant1–Ant8) into the metal bezel of the smartphone to form an 8-antenna array for a sub-6 GHz 8×8 MIMO system. Note that each antenna unit is a slot antenna type consisting of a Chinese character " "-shaped slot and a 50 Ω microstrip feeder, and satisfactory impedance matching is achieved in the upper-frequency band by loading a tuning stub on the feeder. The proposed antenna array successfully covers the required frequency band (2.03–5.21 GHz), corresponding to the N77/N78/N79 and Wi-Fi 2.4 GHz frequency bands for 5G. Consequently, key performance indicators are distinguished, including the rejection of mutual coupling (< −10 dB), acceptable overall antenna efficiency (73%–75%), exceptional envelope correlation coefficient (< 0.01), and excellent far-field radiation patterns.

ACKNOWLEDGMENT

This work was supported in part by the Anhui Provincial Natural Science Foundation of China under Grant 2108085MF200, in part by the Natural Science Foundation of Anhui Provincial Education Department under Grant No. KJ2020A0307 and No. 2022AH051583, and the Graduate Innovation Fund of Anhui University of Science and Technology under grant No. 2022CX2082.

REFERENCES

1. Kulkarni, J., J.-Y. Chen, T.-Y. Zhang, and C.-Y.-D. Sim, "A broadband 8-antenna array design for 5G MIMO smartphone applications," *2021 International Symposium on Antennas and Propagation (ISAP)*, 1–2, Taipei, Taiwan, 2021.
2. Peng, H., R. Zhi, Q. Yang, J. Cai, Y. Wan, and G. Liu, "Design of a MIMO antenna with high gain and enhanced isolation for WLAN applications," *Electronics*, Vol. 10, No. 14, 1659, 2021.
3. Dharmarajan, A., P. Kumar, and T. J. O. Afullo, "A high gain UWB human face shaped MIMO microstrip printed antenna with high isolation," *Multimedia Tools and Applications*, 34849–34862, 2022.
4. Kiani, S. H., A. Altaf, M. R. Anjum, et al., "MIMO antenna system for modern 5G handheld devices with healthcare and high rate delivery," *Sensors*, Vol. 21, No. 21, 7415, 2021.
5. Chen, H.-D., Y.-C. Tsai, C.-Y.-D. Sim, and C. Kuo, "Broadband eight-antenna array design for sub-6 GHz 5G NR bands metal-frame smartphone applications," *IEEE Antennas and Wireless Propagation Letters*, Vol. 19, No. 7, 1078–1082, 2020.
6. Ren, Z., S. Wu, and A. Zhao, "Triple band MIMO antenna system for 5G mobile terminals," *2019 International Workshop on Antenna Technology (iWAT)*, 163–165, Miami, FL, USA, 2019.
7. Serghiou, D., M. Khalily, V. Singh, A. Araghi, and R. Tafazolli, "Sub-6 GHz dual-band 8×8 MIMO antenna for 5G smartphones," *IEEE Antennas and Wireless Propagation Letters*, Vol. 19, No. 9, 1546–1550, 2020.
8. Hei, Y. Q., J. G. He, and W. T. Li, "Wideband decoupled 8-element MIMO antenna for 5G mobile terminal applications," *IEEE Antennas and Wireless Propagation Letters*, Vol. 20, No. 8, 1448–1452, 2021.
9. Parchin, N. O., H. J. Basherlou, I. A. Yasir Al-Yasir, M. Sajedin, J. Rodriguez, and R. A. Abd-Alhameed, "Multi-mode smartphone antenna array for 5G massive MIMO applications," *2020 14th European Conference on Antennas and Propagation (EuCAP)*, 1–4, 2020.
10. Ban, Y.-L., C. Li, C.-Y.-D. Sim, G. Wu, and K.-L. Wong, "4G/5G multiple antennas for future multi-mode smartphone applications," *IEEE Access*, Vol. 4, 2981–2988, June 21, 2016.
11. Jha, P., A. Kumar, A. De, and R. K. Jain, "Modified CSRR based dual-band four-element MIMO antenna," *Progress In Electromagnetics Research Letters*, Vol. 101, 35–42, 2021.
12. Jiang, W., B. Liu, Y. Cui, and W. Hu, "High-isolation eight-element MIMO array for 5G smartphone applications," *IEEE Access*, Vol. 7, 34104–34112, 2019.
13. Zhao, A. and Z. Ren, "Wideband MIMO antenna systems based on coupled-loop antenna for 5G N77/N78/N79 applications in mobile terminals," *IEEE Access*, Vol. 7, 93761–93771, 2019.
14. Zhao, X., S. P. Yeo, and L. C. Ong, "Decoupling of inverted-F antennas with high-order modes of ground plane for 5G mobile MIMO platform," *IEEE Transactions on Antennas and Propagation*, Vol. 66, No. 9, 4485–4495, 2018.
15. Wong, K.-L., C.-Y. Tsai, and J.-Y. Lu, "Two asymmetrically mirrored gap-coupled loop antennas as a compact building block for eight-antenna MIMO array in the future smartphone," *IEEE Transactions on Antennas and Propagation*, Vol. 65, No. 4, 1765–1778, 2017.
16. Zhao, A. and Z. Ren, "Size reduction of self-isolated MIMO antenna system for 5G mobile phone applications," *IEEE Antennas and Wireless Propagation Letters*, Vol. 18, No. 1, 152–156, 2019.
17. Chen, S.-C., L.-C. Chou, C.-I. G. Hsu, and S.-M. Li, "Compact sub-6-GHz four-element MIMO slot antenna system for 5G tablet devices," *IEEE Access*, Vol. 8, 154652–154662, 2020.
18. Parchin, N. O., et al., "Eight-element dual-polarized MIMO slot antenna system for 5G smartphone applications," *IEEE Access*, Vol. 7, 15612–15622, 2019.
19. Li, Y., C.-Y.-D. Sim, Y. Luo, and G. Yang, "High-isolation 3.5 GHz eight-antenna MIMO array using balanced open-slot antenna element for 5G smartphones," *IEEE Transactions on Antennas and Propagation*, Vol. 67, No. 6, 3820–3830, 2019.

20. Barani, I. R. R., K.-L. Wong, Y.-X. Zhang, and W.-Y. Li, "Low-profile wideband conjoined open-slot antennas fed by grounded coplanar waveguides for 4×4 5G MIMO operation," *IEEE Transactions on Antennas and Propagation*, Vol. 68, No. 4, 2646–2657, 2020.
21. Zhao, X., S. P. Yeo, and L. C. Ong, "Decoupling of inverted-F antennas with high-order modes of ground plane for 5G mobile MIMO platform," *IEEE Transactions on Antennas and Propagation*, Vol. 66, No. 9, 4485–4495, 2018.
22. Ullah, R., S. Ullah, R. Ullah, F. Faisal, I. B. Mabrouk, and M. J. A. Hasan, 'A 10-ports MIMO antenna system for 5G smart-phone applications," *IEEE Access*, Vol. 8, 218477–218488, 2020.
23. Jaglan, N., S. D. Gupta, and M. S. Sharawi, "18 element massive MIMO/diversity 5G smartphones antenna design for sub-6 GHz LTE bands 42/43 applications," *IEEE Open Journal of Antennas and Propagation*, Vol. 2, 533–545, 2021.
24. Yuan, X.-T., W. He, K.-D. Hong, C.-Z. Han, Z. Chen, and T. Yuan, "Ultra-wideband MIMO antenna system with high element-isolation for 5G smartphone application," *IEEE Access*, Vol. 8, 56281–56289, 2020.
25. Desai, A., T. Upadhyaya, M. Palandoken, and C. Gocen, "Dual band transparent antenna for wireless MIMO system applications," *Microw. Opt. Technol. Lett.*, Vol. 61, 1845–1856, 2019.
26. Li, M., Z. Xu, Y. Ban, Q. Yang, and Q. Zhou, "Eight-port dual-polarized MIMO antenna for 5G smartphone applications," *2016 IEEE 5th Asia-Pacific Conference on Antennas and Propagation (APCAP)*, 195–196, 2016.
27. Dong, J., X. Yu, and L. Deng, "A decoupled multiband dual-antenna system for WWAN/LTE smartphone applications," *IEEE Antennas and Wireless Propagation Letters*, Vol. 16, 1528–1532, 2017.
28. Wang, Y. and Z. Du, "A wideband printed dual-antenna with three neutralization lines for mobile terminals," *IEEE Transactions on Antennas and Propagation*, Vol. 62, No. 3, 1495–1500, 2014.
29. Zhao, A. and Z. Ren, "Multiple-input and multiple-output antenna system with self-isolated antenna element for fifth-generation mobile terminals," *Microwave and Optical Technology Letters*, Vol. 61, No. 1, 20–27, 2019.
30. Fu, Z. and W. Shen, "Eight-element self-decoupled MIMO antenna design for 5G smartphones," *International Journal of RF and Microwave Computer-Aided Engineering*, Vol. 31, No. 3, Art. No. e22523, 2021.
31. Wong, K., C. Wan, and L. Chen, "Self-decoupled compact metal-frame LTE MIMO antennas for the smartphone," *Microwave and Optical Technology Letters*, Vol. 60, No. 5, 1170–1179, 2018.
32. Dubazane, S. P., P. Kumar, and T. J. O. Afullo, "Metasurface superstrate-based MIMO patch antennas with reduced mutual coupling for 5G communications," *The Applied Computational Electromagnetics Society Journal (ACES)*, Vol. 37, No. 4, 408–419, 2022.
33. Bhatia, S. S. and N. Sharma, "Modified spokeswheel shaped mimo antenna system for multibandand future 5G applications: Design and measurement," *Progress In Electromagnetics Research C*, Vol. 117, 261–276, 2021.
34. Jafri, S. I., R. Saleem, M. F. Shafique, and A. K. Brown, "Compact reconfigurable multiple-input-multiple-output antenna for ultra wideband applications," *IET Microwaves, Antennas & Propagation*, Vol. 10, 413–419, 2015.
35. Gurjar, R., D. K. Upadhyay, B. Kanaujia, and A. Kumar, "A compact U-shaped UWB-MIMO antenna with novel complementary modified minkowski fractal for isolation enhancement," *Progress In Electromagnetics Research C*, Vol. 107, 81–96, 2021.
36. Gurjar, R., D. K. Upadhyay, B. K. Kanaujia, and A. Kumar, "A compact modified Sierpinski carpetfractal UWB MIMO antenna with square-shapedfunnel-like ground stub," *AEU — International Journal of Electronics and Communications*, Vol. 117, 153–126, 2020.
37. Chandel, R., A. K. Gautam, and K. Rambabu, "Tapered fed compact UWB MIMO-diversity antenna with dual band-notched characteristics," *IEEE Transactions on Antennas and Propagation*, Vol. 66, No. 4, 1677–1684, 2018.